Modeling the process of optical characteristics variation for a solar sail surface during heliocentric flights

O.L. Starinova[1], M.A. Rozhkov[1], B. Alipova[1,2], I.V. Chernyakina[1]

[1]Samara National Research University, Moskovskoe Shosse 34A, Samara, Russia, 443086
[2]The International Information Technology University, Manas Str. 34/1, Almaty, Republic of Kazakhstan, 050040

Abstract. The changing of optical characteristics for the solar sail surface during the heliocentric flights is considered. The sail surface is a multilayer epitaxial structure, which is physically a polyamide film, covered with different metals from the front and back sides. Optical characteristics of the multilayer film are calculated by the transition matrix method adapted for quantum-sized layers taking into account the solar radiation spectrum. We model the influence of these characteristics on the acceleration of a spacecraft with a solar sail.

1. Introduction

Currently, one of the most promising ways of outer space exploration is by means of a solar sail, which is a spacecraft with a thin mirror film of a large area. Since the solar radiation puts pressure on the film, the solar sail can move in space without wasting any propellant unlike a spacecraft with jet engines. Possible areas of the solar sail application are quite diverse: from geocentric maneuvers to interplanetary and even interstellar flights [1–9].

The development of new technologies makes possible the solar sail implication and evokes practical interest on the part of researchers from different countries. In particular, the problems associated with the optimal control of the geo and heliocentric motion of spacecraft with a perfectly reflective solar sail, the calculation of the corresponding motion paths and sail orientation angles relative to the sun's rays were investigated [10-14]. At the moment, several solar sails projects have been successfully implemented, such as Russian Znamya-2 (1993) [1], Japanese IKAROS (2010) [8], American NanoSail-D2 (2010) [4] and LightSail (2015) [14].

However, in practice the surface of the sail is not perfectly reflective. The flux of solar electromagnetic radiation that falling on the sail surface is partially reflected, dissipated and absorbed by the sail material. In optics this ratio is described by the reflection, dissipation, and absorption coefficients. The magnitude of these coefficients depends on optical properties and thickness of the sail materials, the wavelength of the incident rays and the surface temperature. Thus, the value and direction of an acceleration produced by a practically possible solar sail substantially depends on optical characteristics and temperature of its surface, as well as on the position of the spacecraft relative to the Sun. This paper studies this dependencies.

2. Mathematical model

2.1. Direction and value of an acceleration produced by the plane solar sail with non-ideal reflectivity considering the temperature variation and sail's degradation

The acceleration produced by the spacecraft with a flat non-ideal reflective sail due to the effect of solar radiation pressure is defined as the sum of two components: directed along the normal to the surface of the sail ($a_\perp$) and parallel to the surface of the sail in the plane passing through the radius vector ($a_{||}$).

$$a_\perp = 2\frac{S_r}{cm}S\cdot\cos\vartheta\cdot\left(a_1\cos\vartheta + a_2\right) \tag{1}$$

$$a_{||} = -2\frac{S_r}{cm}S\cdot\cos\vartheta\cdot a_3\sin\vartheta \tag{2}$$

$$a_1 = \frac{1}{2}\left(1+\varsigma\rho\right),\ a_2 = \frac{1}{2}\left(B_f\left(1-\varsigma\right)\rho + \left(1-\rho\right)\frac{\varepsilon_f B_f - \varepsilon_b B_b}{\varepsilon_f + \varepsilon_b}\right),\ a_3 = \frac{1}{2}\left(1-\varsigma\rho\right), \tag{3}$$

where S_r is a solar electromagnetic radiation flux density per unit area of a sail located at a heliocentric distance r; c is the speed of light; m is the mass of the spacecraft; S is the sail surface area; ϑ is the angle between the direction toward the Sun and the normal to the sail surface (installation angle); ρ is the reflection coefficient; ς is the spectral reflection factor of sail surface that describes the dependence of the surface reflection coefficient on the flux wavelength; ε_f, ε_b are emission coefficients of the front and rear sail surfaces; B_f, B_b are not Lambert coefficients of the front and rear sail surfaces, which describe the angular distribution of the emitted and diffusely reflected photons. For the reflective front solar sail surface a well-reflecting aluminum or beryllium is usually chosen. On the contrary, for the rear surface a well-emitting chrome is usually chosen (to maintain a moderate sail temperature). For example, the paper [10] describes a solar sail project for a flight near the Sun with an aluminized face and chrome-plated back surface of the film. Such solar sail has next optical coefficients:

$$\varsigma = 0.88,\ \varepsilon_f = 0.05,\ \varepsilon_b = 0.55,\ B_f = 0.79,\ B_b = 0.55. \tag{4}$$

Non-ideal reflection off the sail surface leads to several negative effects:
- reducing a value of acceleration produced by the solar radiation pressure;
- narrowing a range of available acceleration angles relative to the direction of light flux;
- increasing an amount of light flux absorbed energy that leads to an increase in the surface temperature and speed-up the degradation process.

If we assume that optical characteristics of sail surface are constant throughout the whole spacecraft operation time, then the steady-state temperature of solar sail can be calculated according to the Stefan-Boltzmann law as [9]

$$T = \left(\frac{S_r}{\sigma_{SB}}\frac{1-\rho}{\varepsilon_f + \varepsilon_b}\cos\vartheta\right)^{1/4}\left(\frac{r_0}{r}\right)^{1/2}, \tag{5}$$

where $\sigma_{SB} = 5.67\cdot 10^{-8}$ W·m^{-2}·K^{-4} is the Stefan-Boltzmann constant.

However, it was shown in [12] that when a sail is heated, its emissivity increases and equation (5) can be written as

$$T = \left(\frac{S_r}{\sigma_{SB}}\frac{1-\rho}{\varepsilon_f + \varepsilon_b}\cos\vartheta\right)^{1/4}\left(\frac{r_0}{r}\right)^{2/5}, \tag{6}$$

At the same time, the surface of sail degrades due to influence of various space factors. In particular, the reflection coefficient worsens and the proportion of absorbed radiation increases accordingly. If we

take into account only the solar radiation, then the change in optical characteristics can be calculated from the parametric dependencies proposed in [10–13]:

$$\frac{p(t)}{p_0} = \begin{cases} \dfrac{1+de^{-\lambda\Sigma(t)}}{1+d} & \text{if } p \in \{\rho,\varsigma\}, \\ 1+d\left(1-e^{-\lambda\Sigma(t)}\right) & \text{if } p = \varepsilon_f, \\ 1 & \text{if } p \in \{\varepsilon_b, B_f, B_b\}, \end{cases} \tag{7}$$

where $\Sigma(t)$ is the dimensionless total dose of solar radiation received during the flight; λ is the coefficient of degradation; d is the degradation factor. The dimensionless total dose of solar radiation is calculated as the ratio of the total radiation power received by the sail during the flight to the solar radiation power received by the 1 m^2 area at a distance of 1 AU during one year $\tilde{\Sigma}_0 = 15.768 \cdot 10^{12}$ J

$$\Sigma(t) = \frac{\tilde{\Sigma}(t)}{\tilde{\Sigma}_0} = \frac{1}{1 year} \int_{t_0}^{t} \frac{\cos\vartheta(t)}{r^2} dt . \tag{8}$$

The degradation coefficient λ is determined with accordance to half the life time of sail under the influence of solar radiation.

$$\lambda = \frac{\ln 2}{\hat{\Sigma}} , \tag{9}$$

where $\hat{\Sigma}$ is the dose of solar radiation, which leads to deterioration of optical characteristics by half, i.e. corresponds to the value of the optical characteristic $\hat{p} = \dfrac{p_0 + p_\infty}{2}$.

The degradation factor d determines the value of optical characteristic p_∞ at which the sail should cease to function. Wherein

$$\rho_\infty = \frac{\rho_0}{1+d}, \ \varsigma_\infty = \frac{\varsigma_0}{1+d}, \ \varepsilon_{f\infty} = \varepsilon_{f0}(1+d). \tag{10}$$

Even a preliminary analysis of the equations (1-10) shows that the acceleration from the solar sail and, consequently, sail control laws and corresponding trajectories of motion depend on optical characteristics of surface. In turn, optical characteristics depend on control laws and flight trajectories. Therefore, a comprehensive analysis of possible interplanetary missions of the spacecraft with a solar sail requires consideration of all listed interrelated parameters.

2.2. Calculation of optical characteristics for the solar sail made of a reflective film with given design parameters

Another problem is to determinate optical characteristics of a film from which the solar sail will be manufactured and to choice suitable surface materials. The film from which solar sails are made has a thickness in the order of several microns and it is sprayed by metallic reflective and radiant surfaces with the thickness of several nanometers. Thus, the solar sail is a multilayer epitaxial structure containing quantum-dimensional layers. Ground testing of film samples is difficult, since the solar spectrum is significantly different on the Earth's surface from the interplanetary space. Under the protection of the Earth's atmosphere, high-energy zones of the spectrum are lost, which in space can significantly influence the behavior of solar sail.

To calculate optical characteristics of a multilayer solar sail film in case of a given wavelength radiation, we use the transition matrix method [15] based on the description of electromagnetic field by two linearly independent components, which are the electric and magnetic fields connected by the transition matrix. The transition matrix through the entire layered structure $\mathbf{M}_\Sigma$ is equal to the product of transition matrices through separate layers $\mathbf{M}_i$, starting with the illuminated (front) surface of the

solar sail. In a non-magnetic environment (in the case of an S-polarized wave) the transition matrix is determined by the expression

$$\mathbf{M}_i^S(\omega) = \begin{pmatrix} \cos f_i & \dfrac{-i}{n_i \cos \theta_i} \sin f_i \\ -in_i \cos \theta_i \sin f_i & \cos f_i \end{pmatrix}, \tag{11}$$

$$f_i = k_0 n_i d_i \cos \theta_i, \ \ k_0 = \omega/c, \tag{12}$$

where f_i is the phase accumulated by the wave when moving from one layer boundary to another, k_0 is the wave vector of light, ω is the cyclic frequency of light, d_i is the layer thickness, n_i is the complex refractive index, θ_i is the angle of light propagation in the layer, which is related to the incident on the structure angle θ_0 by the Snell's law .

In the case of a P-polarized wave, equation (7) takes the form

$$\mathbf{M}_i^P = \begin{pmatrix} \cos f_i & \dfrac{-in_i}{\cos \theta_i} \sin f_i \\ \dfrac{-i \cos \theta_i}{n_i} \sin f_i & \cos f_i \end{pmatrix}. \tag{13}$$

The reflection and transmission energy coefficients of all layers are calculated by the equations

$$\rho(\omega) = |r(\omega)|^2, \ \ r(\omega) = \frac{\left(M_{11}^{S,P} + M_{12}^{S,P} p_l\right) p_0 - \left(M_{21}^{S,P} + M_{22}^{S,P} p_l\right)}{\left(M_{11}^{S,P} + M_{12}^{S,P} p_l\right) p_0 + \left(M_{21}^{S,P} + M_{22}^{S,P} p_l\right)}, \tag{14}$$

$$\tau(\omega) = \frac{p_1}{p_0} |t(\omega)|^2, \ \ t(\omega) = \frac{2 p_0}{\left(M_{11}^{S,P} + M_{12}^{S,P} p_l\right) p_0 + \left(M_{21}^{S,P} + M_{22}^{S,P} p_l\right)}, \tag{15}$$

where for S-polarized light $p_0 = n_0 \cos \theta_0$ and for P-polarized light $p_l = n_l \cos \theta_l$. Instead of p_0 and p_l in equations (14-15) it is necessary to substitute $q_0 = \cos \theta_0 / n_0$ and $q_l = \cos \theta_l / n_l$ respectively.

The complex refractive indices of the material in equations (11–14) depend on the frequency of the incident light. Experimental data published in the form of a public database on the website [16] were used as initial data for calculations. To calculate optical characteristics of the sail surface, which is under the action of the solar radiation entire spectrum, the following equation that actually averaging the reflection and transmission coefficients and taking into account the spectral intensity of solar radiation was used:

$$\hat{\rho} = \frac{\int_{\omega_0}^{\omega_1} Si(\omega) \rho(\omega) d\omega}{S_r}, \ \ \hat{\tau} = \frac{\int_{\omega_0}^{\omega_1} Si(\omega) \tau(\omega) d\omega}{S_r}, \tag{16}$$

where $Si(\omega)$ is the intensity of given solar radiation wave, which is considered as a constant for a given distance from the Sun and calculated according to the data of work [11].

3. Results

We consider the scenario where direction of the sun's rays coincide with the direction of the abscissa axis, a spacecraft weighing 100 kg uses a sail with an area of 10000 m^2 and flights at a distance of 1 AU from the Sun.

Figure 1 shows the position of the spacecraft acceleration vector end regarding to the light pressure $\mathbf{a} = \left(a_\perp, a_{||}\right)^T$ in the boundary coordinate system when the sail angle is changed. Acceleration from a perfect reflecting sail with a zero installation angle (perpendicular to the direction of solar radiation), which is in dimensional form equal to $a_0 = 2\dfrac{S_r}{cm} S = 0.9107$ mm/s^2, is taken as a unit. The outer line corresponds to the acceleration from the perfectly-reflecting sail ($\rho = 1$). Internal lines correspond to

surfaces with different reflection coefficients (0.95, 0.9, 0.85 and 0.8). The distance from each point of line to the origin of coordinates corresponds to the relative magnitude of acceleration compared to the acceleration of ideally reflecting sail with the same area. Figure 2 shows how the angle between the direction of acceleration varies from the forces of light pressure and the heliocentric radius vector of spacecraft depending on the angle of sail for the same values of reflection coefficient.
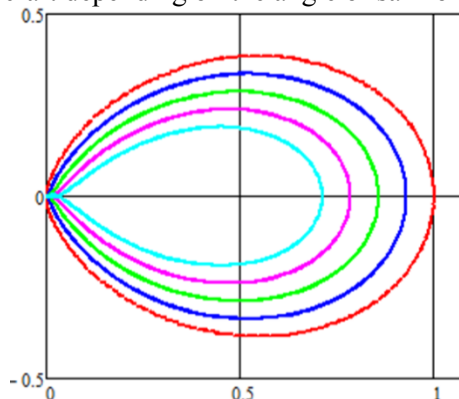

Figure 1. The hodograph of the spacecraft acceleration from the forces of light pressure for different coefficients of reflection.
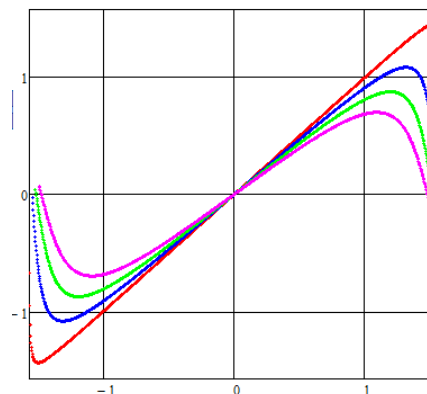
Figure 2. The dependence of the angle between the acceleration direction and the radius-vector from the angle of solar sail.

Figure 3 shows the dependence of the steady-state surface temperature of a solar sail from optical characteristics, which are described by the equation (4). The dependence of the sail temperature (in ° K) from the heliocentric distance toward the spacecraft and the angle of sail, which calculation is shown in the equation (6).

Figure 4 demonstrates the change in the reflection coefficient of the solar sail due to degradation. We assumed that spacecraft performs periodic passive movement in a heliocentric orbit with a pericenter equal to the radius of the orbit of Mercury and an aphelion equal to the average radius of the Earth's orbit. The dependence of the reflection coefficient over 10 years from various factors of degradation is shown. The upper line corresponds to the degradation factor $d = 0,05$ for the sail with the original optical characteristics, as it is described by the equation (4). The bottom lines correspond to degradation factors $d = 0.05, \ 0.10, \ 0.15, \ 0.20, \ 0.25$.

For the calculation of the optical coefficients, a kapton film with a thickness of 3 μm was considered, from the front and back sides of which a layer of aluminum and chromium 60 nm thick was deposited. Figures 5 and 6 show the dependences of the reflection and absorption coefficients from the angle of light incidence on the sail surface for S-polarized (dashed line), P-polarized (dotted line) and non-polarized (solid line) electromagnetic radiation with a wavelength of 300 nm.

As an example of the proposed mathematical model application, we consider the flight of a spacecraft to Mercury using the locally optimal sail control laws described in [14]. The start date of the heliocentric movement is January 25, 2022 and the duration of the heliocentric flight is 315.25 days; the date of reaching Mercury is 5 December, 2022. Motion modeling was carried out in two stages: Stage 1 — the shortest reduction of the major semiaxis as fast as possible (284.75 days); Stage 2 - the most rapid increase in eccentricity (30.5 days). The date of the heliocentric movement beginning was chosen from the condition of the spacecraft entering the planet sphere of action. The main results of the simulation are shown in Table 1 and in Figure 7.

Figure 7 shows the calculated trajectories of the terrestrial planets and the spacecraft controlled motion. Figure 8 shows the change in the steady-state surface temperature of the spacecraft. The lower curve in Figure 8 corresponds to the simulation without taking into account the sail degradation and the upper one is calculated taking into account the change in optical characteristics due to degradation.
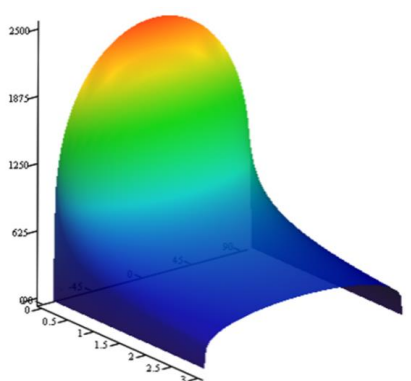
Figure 3. The established surface temperature (K) plotted against the heliocentric distance and the installation angle.
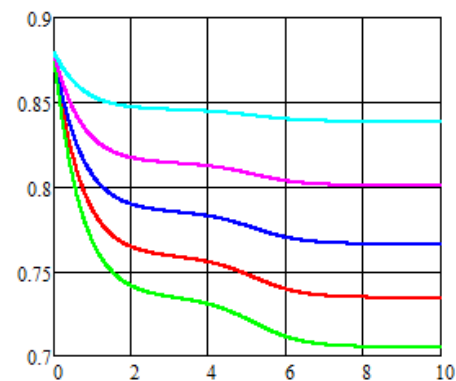

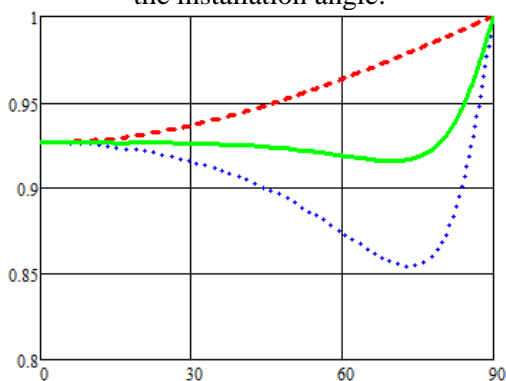**Figure 4.** Change of the sail reflection coefficient during the flight (in years).

Figure 5. The reflection coefficient of the solar sail film depending on the angle of incidence of sunlight.
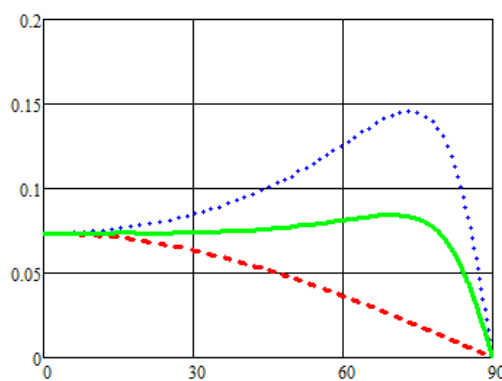

Figure 6. The absorption coefficient of the solar sail film, depending on the angle of incidence of sunlight.

Table 1. Initial data and results of calculation of the basic flight to Mercury.

Mission parameter	Value
The initial mass of the spacecraft, kg	100
The Sail area, m^2	10000
The coefficient of the front sail surface (Al) mirror reflection	0.88
The coefficient of the front sail surface (Al) secondary radiation	0.05
The coefficient of the rear sail surface (Cr) secondary radiation	0.55
Escape from Earth	25.01.2022
The duration of stage 1 – reduction of the major semiaxis, days	284.75
Start date of the stage 2	5.11.2022
The duration of stage 2 – reduction of the orbit eccentricity, days	30.5
Date of reaching the target orbit	5.12.2022
Maximum established surface temperature of the sail Al/Cr, °K (excluding degradation / taking into account degradation of the sail)	378 / 403

4. Conclusion

The article describes the method developed by the authors for calculating the initial optical properties of the sail surface, their variation as a result of sail degradation and changes in surface temperature. We also consider the effect on dynamic parameters of the spacecraft motion, allowing for a refined design and ballistic analysis of interplanetary missions powered by a solar sail. As an example, the calculation of the flight to Mercury were made.
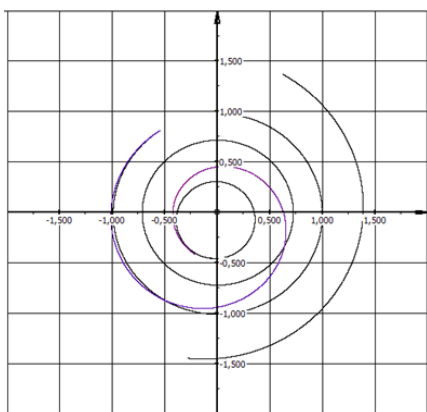
Figure 7. The flight trajectory of the spacecraft with a solar sail, which has given characteristics, to Mercury.
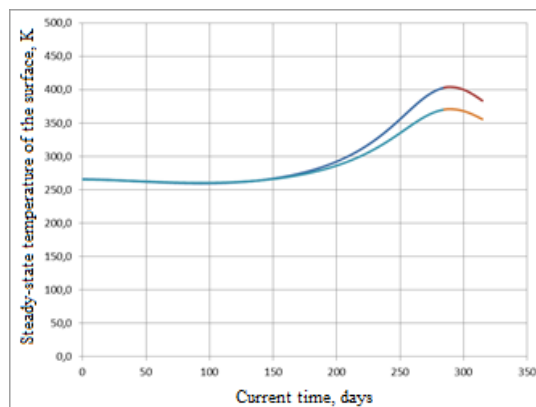

Figure 8. Comparison of the steady-state surface temperature of the solar sail with and without consideration of the sail degradation. The change of the curve color corresponds to a transition from the first to the second stage of flight.

5. References

[1]   Polyakhova, E.N. Cosmic Flight with Solar Sail. – Moscow: Nauka, 1988. (in Russian).

[2]   Macdonald, M. Solar Sailing: Applications and Technology Advancement / M. Macdonald // Advances in Spacecraft Technologies. – 2011. – P. 35-60.

[3]   Merikallio, S. Moving an asteroid with electric solar wind sail / S. Merikallio, P. Janhunen // Astrophysics and Space Sciences Transactions (ASTRA). – 2010. – Vol. 6(1). – P. 41.

[4]   Friedman, L. Evolutionary lightsailing missions for the 100-year starship / L. Friedman, D. Garber, T. Heinsheimer // Journal of the British Interplanetary Society. – 2013. – Vol. 66. – P. 252-259.

[5]   Staehle, R. Interplanetary CubeSats: opening the solar system to a broad community at lower cost / R. L. Staehle, B. Anderson, D. Betts, D. Blaney, C. Chow, L. Friedman, H. Hemmati, D. Jones, F. Klesh, P. Liewer, J. Lazio, M. Lo, P. Mouroulis, N. Murphy, P. J. Pingree, J. Puig-Suari, T. Svitek, A. Williams, T. Wilson // Journal of small satellites. – 2013. – Vol. 2(1). – P. 161-186.

[6]   Matloff, G. L. Solar sail starships: the clipper ships of the galaxy / G. L. Matloff, E. Mallove // Journal of the British Interplanetary Society. – 1981. – Vol. 34. – P. 371-380.

[7]   Vulpetti, G. Solar sails: a novel approach to interplanetary travel / G. Vulpetti, L. Johnson, G. L. Matloff. – Springer, 2014.

[8]   Tsuda, Y. Flight status of IKAROS deep space solar sail demonstrator / Y. Tsuda, O. Mori, R. Funase, H. Sawada, T. Yamamoto, T. Saiki, J.I. Kawaguchi // Acta Astronautica. – 2011. – Vol. 69(9-10). – P. 833-840.

[9]   Koblik, V.V. Controlled sailed transfer into circum-solar orbits with constraints on the solar sail temperature / V. V. Koblik, E.N. Polyakhova, L.L. Sokolov, A.S. Smirnov // Space Researches. – 1996. – Vol. 34(6). – P. 618-625. (in Russian).

[10]   Dachwald, B. Impact of optical degradation on solar sail mission performance / B. Dachwald, M. Macdonald, C. R. McInnes, G. Mengali, A. A. Quarta // Journal of Spacecraft and Rockets. – 2007. – Vol. 44(4). – P. 740-749.

[11]   Kezerashvili, R.Ya. Solar Radiation and the Beryllium Hollow-Body Sail-1. The Ionization and Disintegration Effects / R.Ya. Kezerashvili, G. L. Matloff // Journal of the British Interplanetary Society. – 2007. – Vol. 60. – P. 169-179.

[12]   Kezerashvili, R.Ya. Solar sail: materials and space environmental effects / R. Ya. Kezerashvili // Advances in Solar Sailing. – Springer, Berlin, Heidelberg, 2014. – P. 573-592.

[13]   Dachwald, B. Parametric model and optimal control of solar sails with optical degradation / B. Dachwald, M. Macdonald, C.R. McInnes, G. Mengali, A.A. Quarta // Journal of Guidance, Control, and Dynamics. – 2006. – Vol. 29(5). – P. 1170-1178.

[14] Starinova, O.L. The Mission's Design of a Solar Sail Spacecraft to the Nearest Circumsolar Space, Based on Local-optimal Control Laws / O. L. Starinova, I.V. Chernyakina // Advances in Astronautics Science and Technology. – 2018. – Vol. 1(1). – P. 81-85.

[15] Principles of Optics / M. Born, E. Wolf. – Cambridge University Press, Cambridge, 1999. – 952 p.

[16] Refractive index database [Electronic resource]. – Access mode: https://refractiveindex.info/.